Identification of BRDF parameters with spectral measurements in the visible light spectrum towards solar irradiation evaluation in urban environment for photovoltaïc technologies

Blaise Raybaud, Etienne Vergnault, Angela Disdier, Philippe Thony, Jean-Jacques Roux

Identification of BRDF parameters with spectral measurements in the visible light spectrum towards solar irradiation evaluation in urban environment for photovoltaïc technologies

Blaise Raybaud[1,2], Etienne Vergnault[2], Angela Disdier[1], Philippe Thony[1], Jean-Jacques Roux[2]
[1]Université Grenoble Alpes, CEA/LITEN, INES, F-38000 Grenoble, France
[2]Université de Lyon, INSA-Lyon, CETHIL UMR5008, F-69621 Villeurbanne, France

Abstract

In order to incorporate real construction material reflectance properties in a Monte-Carlo ray tracing algorithm, a representative cladding material is characterised with a spectrophotometer to obtain reflectance angular distribution. These measurements are used to design a BRDF model with a reduced number of parameters that are further identified, along with their confidence intervals. Obtained results are compared to reflectance coefficients measured with an integrating sphere. The prospects of such a model is to allow for a more accurate modelling of the optical properties of materials in reflection. This knowledge can then allow a better integration of photovoltaic technologies, both in terms of energy and visual acceptance. For the particular HPL cladding material tested and despite a highly specular behavior at grazing incidence angles, we found that the specular term only amounts to 4% of reflection.

CRediT. Blaise Raybaud (Formal analysis, Data Curation, Writing),
Etienne Vergnault (Methodology, Writing - Review & Editing),
Angela Disdier (Measurement),
Philippe Thony (Funding acquisition, Supervision, review, writing),
Jean-Jacques Roux (Supervision)

Keywords: BRDF, Ray tracing simulation, Building integrated photovoltaic facade, Urban energy simulation, Urban facade, Optical

Contents

1. Nomenclature

- θ_o: Angle of measurement.
- θ_i: Angle of incidence.
- $\theta_{mes,ini}$: First angle for which a measurement in reflection is carried out (at fixed angle of incidence).
- $\theta_{mes,fin}$: Last angle for which a measurement in reflection is carried out (at fixed angle of incidence).
- θ_{step}: Angular measurement pitch with the ARTA.
- N: number of measurements performed (at fixed angle of incidence).
- φ_o: Angle in which the observer is located in the plane of the sample, in relation to the axis $\vec{y}$.
- φ_i: Angle of the incidence ray in the plane of the sample, in relation to the axis $\vec{y}$.
- L_o: Radiance (power by unit area of reflecting material per unit solid angle of observer) [Wsr^{-1}m^{-2}].
- L_i: Radiance (power by unit area of reflecting material per unit solid angle of light source) [Wsr^{-1}m^{-2}].
- E_i: Irradiance (power per unit area at reflecting material surface) [Wm^{-2}].
- E_{i_0}: Irradiance (power per unit area of incident beam cross-section) [Wm^{-2}].
- I_o: Reflected radiant intensity [W/sr].
- I_o^s: Specular component of the reflected radiant intensity [W/sr].
- I_o^s: Diffuse component of the reflected radiant intensity [W/sr].
- M_o: Outgoing power of reflecting material [W].
- M_i: Incident power on reflecting material [W].
- R_x: reflection coefficients for the x^{th} polarization from the Fresnel's law.
- $f_r(\theta_i, \theta_o, x)$: BRDF function [$sr^{-1}$].
- Z_0: Impedance in vacuum.
- Z_x: Impedance of the x^{th} medium.
- n_x: Refractive index of the x^{th} medium.
- ρ_x: reflection index of the BRDF model, with x the corresponding component (specular or diffused).
- α: Power coefficient of the specular component of the BRDF function.
- k_x: Final reflection indexes obtained from the BRDF model, with x the corresponding component.
- k_g: Global final reflection.
- S_i: Illuminated surface of the sample [m^2].
- $\cos_+(a) = \frac{\cos(a)+|\cos(a)|}{2}$ with $a \in [0 : 2\pi]$

2. Introduction

Studies of solar potential in urban environments are today mostly useful for numerous applications in various domain, as local production of solar energy in urban areas [1], access to natural light towards better life experience of citizen [2] or simulation of radiative transfer in visible and thermal spectral ranges to avoid overheating in districts (radiative trapping at district scale, redistribution of energy). These numerical studies have different objectives: to assess the solar potential for photovoltaic energy conversion [3, 4], to validate access to natural light in buildings for human comfort and health [5], but also to evaluate the exterior facade temperatures of the various buildings of a dense district [6, 7, 8]. Current simulations of solar light propagation in urban environment are generally based on visual rendering strategies used in graphics rendering. Generally, back reflected light on walls [9] is considered as scattered light without considering the spectral or polarization properties. We also have to distinguish light behaviour and surface properties in at least two spectral ranges: visible light (visual comfort, aesthetics, PV conversion) and thermal radiation (thermal comfort and emissivity, urban heat islands and greenhouse effects). The objective of this study is, firstly, to evaluate the impact of these properties of light for precise energy estimation and, secondly, to take into account the exact nature of light reflections in the visible spectral range (as opposed to thermal spectral range) in order to verify the hypothesis of diffuse light reflection currently assumed in most studies [10]. Raybaud's thesis [11] shows the impact that such patterns can have on the energy distribution within a street. Figure 1 shows the extreme cases, where the reflections are either only diffuse (left figure) or only specular (right figure).

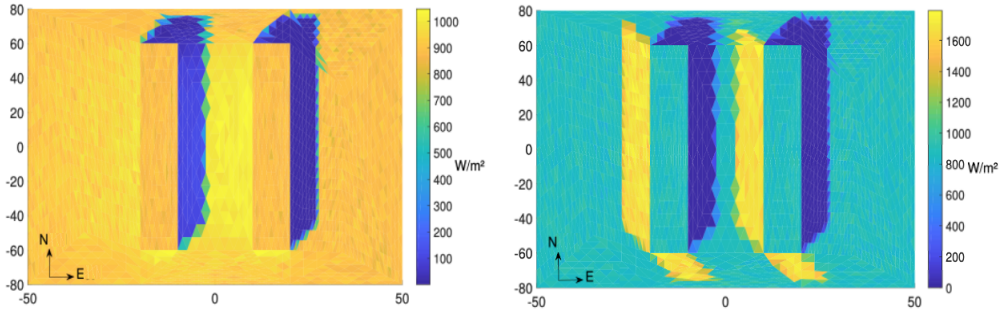

Figure 1: Comparison of energy distributions as a function of reflection mode (diffuse in the left figure; specular in the right figure) (from Raybaud [11])

The study of optical properties leads to select a set of materials and optical behaviour as reflection, transmission, absorption and diffusion. These

properties are described through mathematical functions, whose name often appears in BxDF format for Bidirectional Distribution "x" Function, x standing for a specific optical behaviour. BxDF distribution functions are mainly used in computer graphics rendering [12]. However, these methods are being studied for a better assessment of the impact of the sun on heat transfer in urban areas, in particular for "glass" materials [13] or Hight Reflective Materials (HMRs) used to reduce the Urban Heat Island (UHI) effect [14]. The visual rendering of virtual scenes is similar to solar light and natural lighting studies in urban environments, especially when surface properties are considered. It is then interesting to look at the functions used in the simulation of visual rendering. These functions include in particular: BTDF (transmittance), BRDF (reflectance), BSSRDF (surface scattering in reflection), BSSTDF (surface scattering in transmission) or BSDF (BSSRDF and BSSTDF), as shown on Figure 2. These surface properties depend on incidence and viewing angles, wavelength, polarization, and also local space coordinates. When considering the simulation of light propagation in urban scenes, functions related to the BRDF family are commonly used [15, 13]. Radiance software is a priori the most adapted to take into account such models but the handling is complex [16]. Measuring reflectance data to obtain a realistic BRDF of outdoor environments is also a challenge today [17]. The light reflected on the opaque materials is generally divided into two components: Lambertian retrodiffusion and specular reflection [18]. These distribution functions are also used in yield calculations of bifacial photovoltaic modules [19], with the aim of studying the impact of local environment on the electricity production of the PV modules. Transmission functions (BTDF) are often used to evaluate the effects of glazing on interior lighting [20, 16].

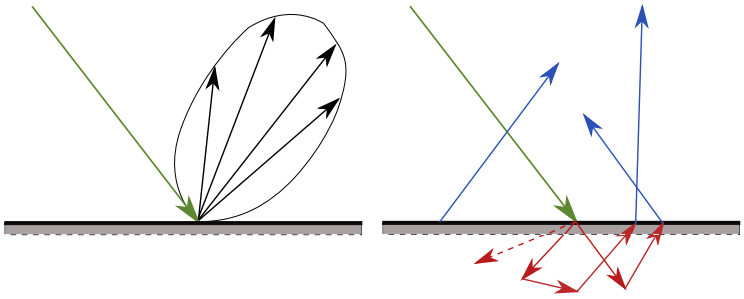

(a) BRDF (b) BSSDF

Figure 2: Illustration of a BRDF and a BSSDF

In addition, Collin et al. emphasize the effects of polarization in reflections [21] for such application. This is particularly true if incident light is described with polarisation vector decomposition in the simulation process,

even if the human eye cannot distinguish light polarization.

Initial work from Phong results in a widely used method for computer generated pictures and visual rendering modelling [22]. This approach is based on the reconstruction of the scene in the direction of the viewer, with contributions from specular and diffused light, as is the Lafortune model [23]. The Blinn-Phong model [24] proposes a different formulation by including the consideration of the local nature of the surface with micro-facets. This model therefore corresponds well to a BRDF and thus ensures energy conservation. However, the specular term can become difficult to standardize. This depends in particular on the function of the chosen specular term [24]. Other models have thus been progressively developed in order to better take into account the specular reflection. The surface roughness of the materials and then the polarization of light were also integrated into the models. The model from Cook-Torrance-Sparrow [25, 26] is the first physical rendering BRDF model. The surface is assimilated to a set of elementary mirror surfaces respecting Fresnel's laws [27]. Under these assumptions, the model corresponds to a statistical distribution of the orientation of the set of surfaces. Several other models are based on a theory of micro facets, like [28]. Studies of solar potential in urban areas often use strong assumptions for reflection models while BRDF can encompass much more details but are sometimes impractical for ray tracing algorithms. We aim at designing a BRDF for solar potential evaluation that is suitable for ray tracing and at identifying its coefficients from spectrophotometry measurements.

The first part of this article presents the global methodology used for solar energy evaluation and more precisely, for the integration of measured optical surface properties. Then, Section 2 presents some classical BRDF models, their limitations regarding our objectives and the hypotheses, parameters and model used in this article, as long as the measurement methodology and model fitting strategy. The third section displays reflection's results obtained with the spectrophotometer on a selected cladding material sample (a white manufactured High Pressure Laminate (HPL)) panel with color coating: the identified BRDF is compared to reference reflection coefficients. Then, Section 4 discusses the use of the proposed BRDF in a Ray-Tracing solar irradiation evaluation code and compares simulation results with experimental data on the same setup. Lastly, this study is concluded and some directions for future research are proposed.

3. Methodology

Overall methodology for solar irradiation evaluation. The aim of this work is to implement real properties of light reflection in solar energy evaluations but without complex light electromagnetic description. This approach was

motivated by the optical reflection characterisation of several real construction materials. These measurements are analysed through models as simple and realistic as possible, and then used to feed a radiative transfer simulation tool. Analogous to existing irradiance models, a ray tracing method based on Monte Carlo statistical sampling allows us to calculate the incident flux in the visible wavelength range (380nm to 740nm). To get an efficient implementation of reflection properties in the ray tracing calculations, an integration of the reflections using Bidirectional Reflectance Distribution Functions (BRDF) is desired. However, for easy integration, it is necessary to reduce the number of parameters describing BRDF model. This will ensure rapid calculations when we will consider wide and dense urban areas for precise solar energy evaluation. Mainly used for computer graphic rendering, usual BRDF models are sometimes not strictly compliant with optical laws or are not physically sound for calculating heat transfer in the mid and far infrared spectral range.We choose here to build the BRDF function in the visible range combining specular and diffuse optical behaviors, making sure that light energy is conserved during reflection and propagation.

The BRDF model proposed in this article is intended to be integrated into the chain of calculation of solar radiation in urban areas (Figure 3). When simulating solar radiation, the optical properties of the materials are often neglected and only one coefficient like the albedo is taken into account. The BRDF integration should allow a better evaluation of the geometric distribution of reflections.

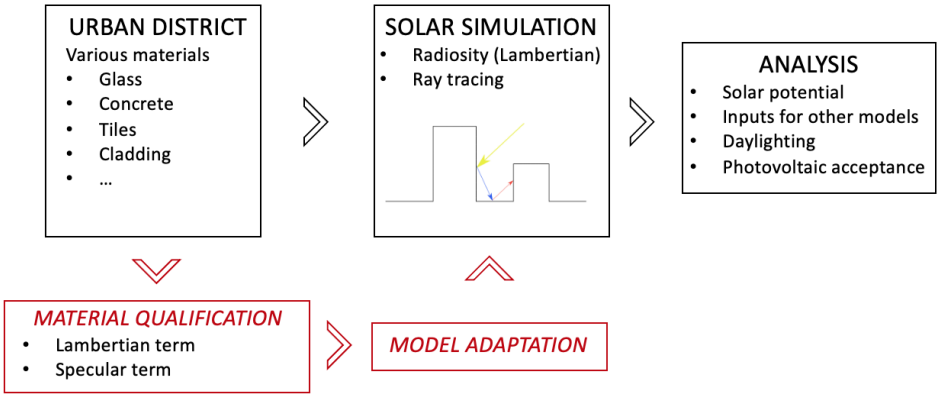

Figure 3: Evaluation strategy for simulating improved urban solar radiation taking into account the BRDF.

Methodology for BRDF Identification. The measurements are carried out with a Lambda 950 UV-VIS spectrophotometer from Perkin Elmer, with a motor driven goniometer allowing full angular reflectance analysis (Automated Reflectance Transmittance Analyzer - ARTA) [29]. The measured spectral range goes from 300nm to 1500nm, wider than the visible spectral

range. Despite using only the visible portion of the spectrum to compute reflection coefficients, the whole available range of wavelength is displayed on the graphics. The identification of a physical model, and mainly of the characteristics of the specular lobe, is complicated by the relatively large opening window of the optical sensors used in the ARTA device. This is dealt with later, see Equation 22. We integrate as many characteristics of the sensors as possible in our calculations when identifying the parameters. However, some assumptions remain: the incident beam in the spectrophotometer is considered as perfectly parallel and the spectral response of the sensors is assumed perfect, which may induce a bias in spectral measurements, as will be discussed in 5.

The following workflow (Figure 4) summarises the approach proposed in this article:

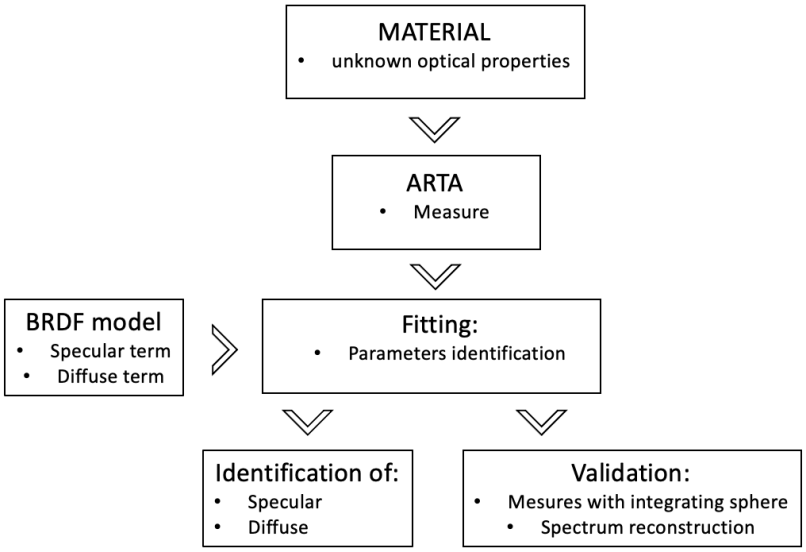

Figure 4: Workflow of the approach proposed in this article.

3.1. Requirements for a BRDF to be used in urban solar irradiation simulations

Due to the diversity of models proposed in the literature, and taking into account the constraint of a simple model that can be easily integrated into urban solar potential simulations, the following section proposes a new BRDF model inspired by the Blinn-Phong model. Fresnel coefficients are integrated to take into account the effects of light polarization, like what is done, at a much larger scale in [30].

3.1.1. Definition of a BRDF

In the following, a BRDF is defined as a ratio of reflected radiance $\mathrm{d}L_o$ ($\mathrm{Wm^{-2}sr^{-1}}$ [10, 31, 32], power per unit area of reflective material per unit solid angle of observer) observed over an infinitesimal solid angle to incident irradiance $\mathrm{d}E_i$ on the sample ($\mathrm{Wm^{-2}}$, power per unit area of reflective material) :

$$f_r = \frac{\mathrm{d}L_o}{\mathrm{d}E_i}. \tag{1}$$

Other sources use an equivalent different definition, but starting from the emitted radiance $\mathrm{d}L_i$ by a light source:

$$f_r = \frac{\mathrm{d}L_o}{\mathrm{d}L_i \cos\theta_i \mathrm{d}\omega_i}, \tag{2}$$

as the received irradiance is linked to the light source radiance by:

$$\mathrm{d}E_i = \mathrm{d}L_i \cos\theta_i \mathrm{d}\omega_i \tag{3}$$

However, since our goal is a reconstruction of a BRDF from measurements made with a goniospectrophotometer, the incident irradiance $\mathrm{d}E_{i_0}$ (along the direction of the incident beam) is also constant and should not be confused with $\mathrm{d}E_i$, see Fig. 5:

$$\mathrm{d}E_{i_0} = \mathrm{d}L_i \mathrm{d}\omega_i \tag{4}$$

A BRDF function is expressed in $\mathrm{sr^{-1}}$ and describes the angular distribution resulting from the reflection of light reflected on a surface. As detailed above, the optical properties depend on the position of the reflection point and the angular position of the source and the observer. Only spatially uniform functions (uniform surface) are considered here and the dependence is limited to the zenithal incidence angle, θ_i, the azimuthal incidence angle φ_i, the reflected zenithal angle θ_o and the reflected azimuthal angle φ_o. The light polarization x can also be considered:

$$f_r(\theta_i, \varphi_i, \theta_o, \varphi_o, x) = \frac{dL_o(\theta_o, \varphi_o, x)}{dE_i(\theta_i, \varphi_i, x)} \tag{5}$$

The goniospectrophotometer only performs measurements in the plane of incidence (containing both the normal to the plane of the sample and the direction of the incident light, see Figure 5). Using a spherical coordinate system with vertical direction normal to the sample, the dependency of the BRDF on φ_i is not relevant. The dependency on φ_o can be measured

partially, as φ_o is either 0 or π. The BRDF can then be written (omitting the polarization):

$$f_r(\theta_i, \theta_o, \varphi_o) = \frac{dL_o(\theta_o, \varphi_o)}{dE_i(\theta_i)} \tag{6}$$

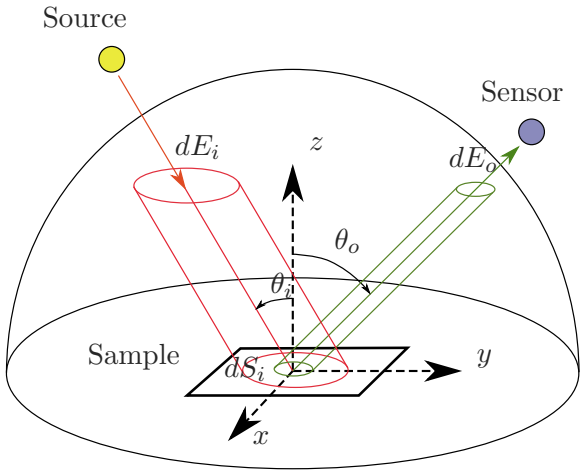

Figure 5: Illustration of the spatial variables used in the article.

According to the definition, a BRDF has to check the two different properties:

- Helmholtz reciprocity:

$$f_r(\theta_i, \varphi_i, \theta_o, \varphi_o) = f_r(\theta_o, \varphi_o, \theta_i, \varphi_i) \tag{7}$$

- Compatibility with energy conservation:

$$\int_{2\pi} f_r(\theta_i, \varphi_i, \theta_o, \varphi_o) \cos\theta_o d\omega_o \leq 1. \tag{8}$$

3.2. BRDF measurements

3.2.1. Measurement protocol

The study presented in this article focuses on a sample of a white exterior cladding material from a recognized brand. In the following, the sample will be called "the sample".

Four different angles of incidence were used: $\theta_{inc} = 20°, 30°, 45°, 55°$. The angle of incidence is noted θ_{inc}.

For each angle of incidence, different angles of measure (θ_o) are used, staggered in steps of $\theta_{step} = 3°$. Because of the physical dimensions of the apparatus, the measurement angle cannot be closer than 15° to the angle of

incidence. Table 6 indicates the number of measurements made for each configuration. The first column titled θ_{inc} corresponds to the angle of incidence of the sample. The columns $\theta_{mes,ini}$ and $\theta_{mes,fin}$ correspond respectively to the minimum and maximum angles (with respect to the direction of incidence) for which a reflectance measurement was made. θ_{step} indicates the measurement angle increment.

θ_{inc}	$\theta_{mes,ini}$	$\theta_{mes,fin}$	θ_{step}
20	*15*	*105*	*3*
30	*15*	*114*	*3*
45	*15*	*126*	*3*
55	*15*	*141*	*3*

Figure 6: Table of different measurement configurations.

3.2.2. Raw measures

In this article, only results obtained with one white cladding material are presented, see Figure 7. A behavior similar to what is discussed below has been observed for other samples, with varying proportions of the diffuse and specular components. On the measurements carried out, the energy distribution measured in reflection appears to be dependent on the S or P polarization of the incident light.

For both polarizations, a diffuse behaviour (the circular part of the curve), mixed with a specular-like one is observed. The intensity of the peaks decreases with the angle of incidence for the P-polarization and increases for the S-polarization. The position of the peak appears to match the theoretical reflection angle given by the Snell–Descartes laws, revealing a geometric effect in the energy distribution.

The amplitude of this reflection presents different attenuation phenomena depending on the polarization. For an increasing angle of incidence, the reflection of the P-polarized light decreases while that of the S-polarized light increases. This observation recalls the laws of geometric optics described by Fresnel. However, this specular effect is not geometrically perfect but appears to be smeared around the theoretical angle of reflection.

3.2.3. Measurements reading

The ARTA measures the fraction r of the energy reflected by the sample that is intercepted by the sensor. This is found (at least for the cladding sample) to depend on the angle on incidence θ_i, the angle of observation θ_o and the polarization of light x. With $\mathrm{d}E_i$ the incident energy ($\mathrm{W/m^2}$) and $\mathrm{d}E_o$ the energy intercepted by the sensor that has an angle of aperture $\mathrm{d}\omega_c$

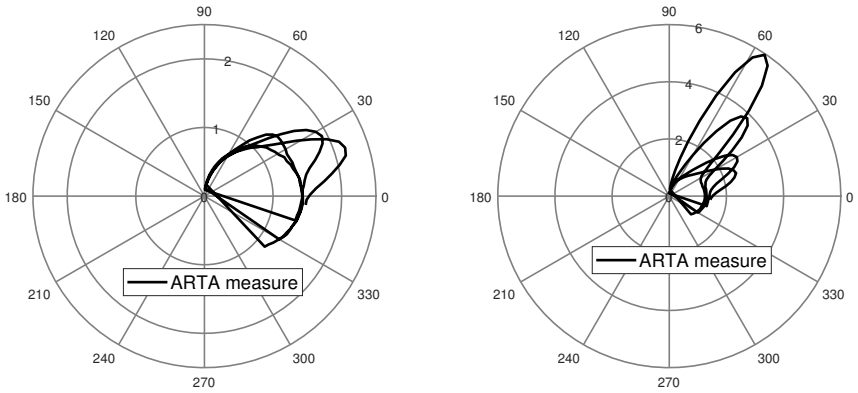

(a) P-polarization (b) S-polarization

Figure 7: Measurements from ARTA: percentage of incident energy reflected by the sample

this is written:

$$r(\theta_i, \theta_o, x) = \frac{\mathrm{d}E_o}{\mathrm{d}E_i} = \frac{\mathrm{d}L_o \mathrm{d}\Omega}{\mathrm{d}E_i} = f_r(\theta_i, \theta_o, x)\mathrm{d}\omega_c. \tag{9}$$

In the following, the link between the BRDF and ARTA measurements is established, then the a model BRDF is built, adapted from the Fresnel equations for the specular part.

3.3. BRDF model construction

In computer graphics, as Kumar [33] points out in his article, it is usual to consider that the light reflection on a given surface is broken down into three modes (Figure (8)). These three terms are a specular term, a uniform term and a bright term. If the reflecting surface is itself a light source, a fourth term is considered. It represents the energy emitted by the surface itself. The uniform component describes the set of non-directional reflections, while the specular and bright components describe the set of reflections with a direction-dependent probability. The term specular describes the reflection resulting from Snell-Descartes laws. This mode of reflection is similar to a Dirac function in the theoretical direction of reflection. The term glossy represents a modulation around this theoretical direction.

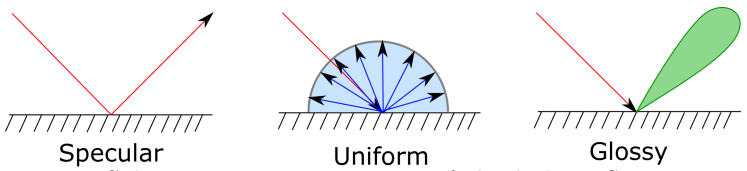

Figure 8: Schematic representation of the light reflection mode.

From the observed behavior, our BRDF model will have a diffuse part and a smeard-specular term, similar to the Blinn-Phong model [24], with the reflected radiant intensity written:

$$I_o = I_o^s + I_o^d. \tag{10}$$

3.3.1. Fresnel equations

Fresnel equations are used to describe the energy distribution of an electromatrical radiation at the interface of two optical materials. These equations detail the difference in polarization for reflected and transmitted energy fluxes. These equations are verified under the following assumptions: the interface between the two media is flat and both media are homogeneous and isotropic. Here, as both media are non-magnetic, their impedances only depend on the refractive indices of the two media ($Z_i = \frac{Z_0}{n_i}$) and the refractive index of air is $n_1 = 1$. Eventually, only the reflectance behaviour is of interest here and writes:

$$R_s(n_2, \theta_i, \theta_o) = \left| \frac{\cos\theta_i - n_2\sqrt{1 - \left(\frac{1}{n_2}\sin\theta_i\right)^2}}{\cos\theta_i + n_2\sqrt{1 - \left(\frac{1}{n_2}\sin\theta_i\right)^2}} \right|^2 \tag{11}$$

$$R_p(n_2, \theta_i, \theta_o) = \left| \frac{\sqrt{1 - \left(\frac{1}{n_2}\sin\theta_i\right)^2} - n_2\cos\theta_i}{\sqrt{1 - \left(\frac{1}{n_2}\sin\theta_i\right)^2} + n_2\cos\theta_i} \right|^2 \tag{12}$$

Although it is not transparent, the sample has an extinction angle : for a given angle of incidence, the P-polarized light is not reflected. This angle, noted θ_B is called the Brewster angle: $\theta_B = \text{atan}(n_2)$. However, in the absence of fine increments in the angle of incidence around the Brewster angle, this relationship is impractical for determining the refractive index n_2 of the sample and in the following, n_2 will be kept as a parameter of our BRDF model.

3.3.2. Model for the smeared-specular term

The specular part is supposed to follow Fresnel's law hence: $\Phi_o^s = k_s R_x \Phi_i$, with R_x the Fresnel reflection coefficient for polarization x. Furthermore, the radiant intensity (W/sr) is supposed be a lobe centered on the specular direction:

$$\mathrm{d}I_o^s(\theta_o, \theta_i, x) = \rho_s R_x \frac{\alpha + 1}{2\pi}\Big(\cos_+(\theta_s)\Big)^\alpha E_i S_i, \tag{13}$$

with θ_s the azimutal angle defined from the specular direction. For values of θ_s larger than $\pi/2$, there is no contribution of specular reflection, as noted by the use of the positive part of the cosine. As in the Lafortune model, the specular term is described by two coefficients ρ_s and α. The coefficient ρ_s corresponds to the magnitude of the specular reflection whereas the coefficient α corresponds to the glossy effect of the specular reflectance and governs the width of the glossy lobe while $\frac{\alpha+1}{2\pi}$ is a ponderation factor. This specular model results in the following BRDF:

$$f_s(\theta_i, \theta_o, x) = \rho_s R_x \frac{\alpha+1}{2\pi} \Big(\cos_+ \Big(\theta_s(\theta_i, \theta_o) \Big) \Big)^{\alpha} \tag{14}$$

3.3.3. Model for the diffuse term

The diffuse term corresponds to the incident light being scattered in all directions, with the same probability and independently of the polarization. However, the radiant intensity depends on the observation angle. This is translated into Lambert's cosine law. A part ρ_d of the incident flux is re-emitted uniformly in all directions:

$$\mathrm{d}I_o^d(\theta_o) = \rho_d \frac{1}{\pi} \cos(\theta_o) E_i S_i, \tag{15}$$

associated with a diffuse part for the BRDF:

$$f_d(\theta_i, \theta_o) = \rho_d \frac{1}{\pi} cos(\theta_o). \tag{16}$$

3.3.4. BRDF model and interpretation of the ARTA outputs

Both modes of reflection a brought together in the following BRDF model:

$$f_r(\theta_i, \theta_o, x) = \rho_d \frac{1}{\pi} cos(\theta_o) + \rho_s R_x \frac{\alpha+1}{2\pi} \Big(\cos_+ \Big(\theta_s(\theta_i, \theta_o) \Big) \Big)^{\alpha}. \tag{17}$$

The ARTA output is a ratio of energy, that is $r = \Phi_o/\Phi_i$. Assuming an infinitesimal angle of aperture $\mathrm{d}\omega_c$, $\Phi_o = I_o \mathrm{d}\omega_c$. The ARTA measurements are performed with the receiver in the plane of incidence, that implies $\theta_s = -\theta_o \cos(\phi_o) - \theta_i$ when $\phi_o = \pi$ and from there:

$$r(\theta_i, \theta_o, \phi_o, x) = \left(\rho_d \frac{1}{\pi} cos(\theta_o) + \rho_s R_x \frac{\alpha+1}{2\pi} \Big(\cos_+(\theta_o - \theta_i) \Big)^{\alpha} \right) \mathrm{d}\omega_c. \tag{18}$$

3.3.5. reflection coefficient calculation

For the two BRDF components and for each polarization, the reflection coefficients are obtained by integrating the BRDF on the upper half-space of

the sample. They depend on the wavelength. Their dependence in polarization and angle of incidence are taken into account through the Fresnel coefficient (Equation 19) :

$$\begin{cases} k_d(x) = \int_{\theta_o=0}^{\pi/2} \int_{\varphi_i=0}^{2\pi} f_d(\theta_i, \theta_o, \phi_o, x) \sin\theta_o \mathrm{d}\theta_o \mathrm{d}\phi_o = \rho_d(x) \\ k_s(\theta_i, x) = \int_{\theta_o=0}^{\pi/2} \int_{\varphi_i=0}^{2\pi} f_s(\theta_i, \theta_o, \phi_o, x) \sin\theta_o \mathrm{d}\theta_o \mathrm{d}\phi_o = \rho_s R_x(\theta_i) \end{cases} \tag{19}$$

The global reflection coefficient is obtained by adding the diffuse and specular reflection coefficients (Equation 20) :

$$k_g(\theta_i, x) = k_d(x) + k_s(\theta_i, x). \tag{20}$$

in order to take both polarizations into account in the global reflection coefficient, the contribution of each polarization is averaged (Equation 21):

$$k_g(\theta_i) = \frac{k_g(\theta_i, S) + k_g(\theta_i, P)}{2}. \tag{21}$$

Those reflection coefficients still depend on the wavelength. When used in Section 5, they are averaged over the visible spectral range.

3.4. Model fitting

3.4.1. Model fitting for a small aperture sensor

To fit the parameters of the BRDF model, a least squares method is used between Eq (18) and the ARTA measures. The model is fitted over the entire set of measurements, i.e. all reflection and incidence angles. Concerning the polarization, the model is approximated either on both polarizations at the same time, or one at a time. The approximation of the model is performed using the Matlab function `lsqcurvefit`. This procedure lead to the identification of the parameters in our BRDF model. However, the smeared-specular term being quite narrow in width and the ARTA sensor having a rather large aperture are in contradiction with Eq (18) therefore it is substituted with a model taking into account the variability of the BRDF over the width of the ARTA sensor.

3.4.2. Correction of the model fitting

In this study, the sensor used by the ARTA has an aperture of $26mm$ in the plane of incidence and the height of this aperture is $18mm$. In this configuration, this corresponds to an aperture ranging from $-13°$ to $+13°$ with respect to the defined measurement angle. Along to the axis orthogonal to the measurement plane, the opening angle is from $-9°$ to $+9°$ with respect to the fixed measurement angle. This gives an opening angle of the

solid-state sensor $\mathrm{d}\omega_c = 0.0516$ sr. The variation of the modelled BRDF over the aperture angle can be taken into account. By minimizing the difference between the theoretical and actual measurements, the calibration of the BRDF model coefficients can be refined. Taking into account the aperture according to the azimuth angle only, the following relation is obtained (Equation 22) :

$$r(\theta_i, \theta_o, \phi_o, x) = \frac{\mathrm{d}\omega_c}{2\Delta\theta} \int_{\theta_o - \Delta\theta}^{\theta_o + \Delta\theta} f_r(\theta_i, \theta, \phi_o, x)\mathrm{d}\theta, \tag{22}$$

This new relationship (22) is used in the model fitting procedure, instead of (18).

3.4.3. Estimating the uncertainties

By performing a non-linear regression, it is possible to evaluate the uncertainties of the parameters of the fitted model, i.e. ρ_s, ρ_p and α, as well as possibly n_2. The use of the function `nlparcy` proposed by Matlab® provides the confidence intervals 95% for each coefficient. By injecting these uncertainties into the coefficient calculations, we can evaluate the uncertainties for the coefficients of the final Lambertian and specular reflections. However, the function `nlparcy` Matlab® requires the covariance matrix or the Jacobian matrix from the BRDF data approximation. A use of the function `nlinfit` (also from Matlab®) is then necessary. For each wavelength, the uncertainties obtained on the different coefficients are propagated in the calculation of the final reflection coefficients.

4. Results: BRDF of a white cladding HPL pannel

4.1. Reference reflection coefficients

In order to verify the results obtained thanks to the BRDF model fitting, the samples are also tested using an integrating sphere mounted in a Lambda 950 Perking Elmer®. This device measures the overall reflection coefficient (diffused plus specular) depending on the wavelength, under an incidence $\theta_i = 8°$. The integrating sphere has an uncertainty of 1%. These measurements are then compared to the global reflection coefficient obtained from the BRDF fitting, as reconstituted using the ARTA measures, for different wavelengths, under the same incidence.

4.2. Results of model fitting

Results by polarization. The obtained BRDF, after model fitting, is plotted for each polarization (Figure 9). However, for the cladding sample, the

differences between corrected and uncorrected models, remain tiny and imperceptible. Concerning the P polarization, and for an angle of incidence of 45°, the model presents difficulties in correctly fitting the measurements. The specular reflection seems to be too important in this configuration only.

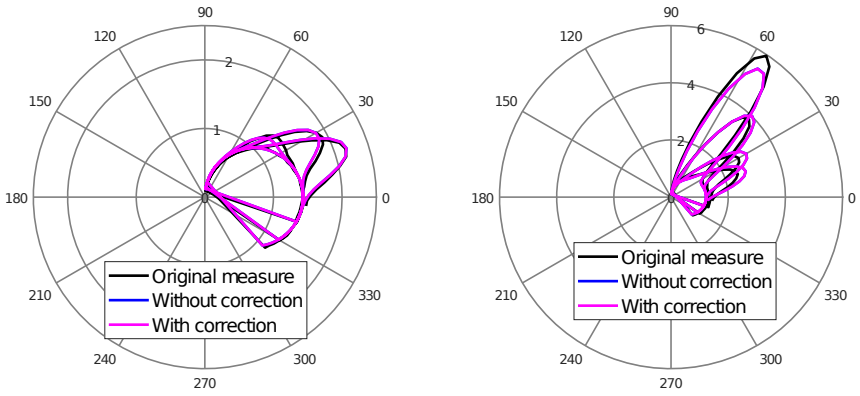

(a) P-polarization (b) S-polarization

Figure 9: Fitted model from the ARTA measurments

The analysis of the reflection coefficients reconstructed from the measurements and the model reveals a sharp change around 860nm. This wavelength corresponds to a sensor change in the ARTA. Depending of the sensor, the global reflection coefficients obtained are either above or below the reflection coefficient obtained with the integrating sphere, especially for the P-polarization. Similar fluctuations depending of the wavelength are observed. These fluctuations are essentially driven by the diffuse coefficient, the specular coefficient being constant over the wavelengths (Figure 10).

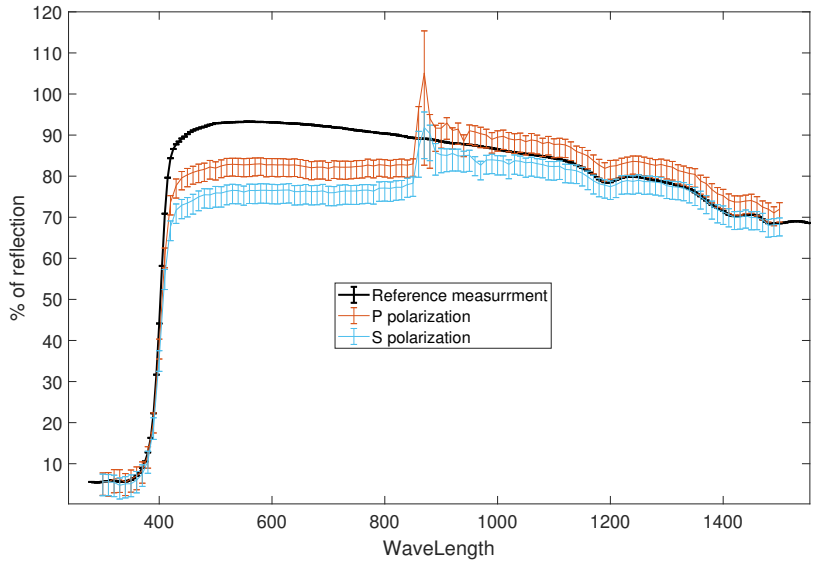

Figure 10: Global reflection coefficients for both polarization depending of the wavelength obtained with the BRDF model, for non corrected and corrected parameters, compared to the Integrating Sphere measures.

Final coefficients. For each wavelength, the model coefficients are approximated. Then, for both non corrected and corrected parameters, the model allows us to obtain the reflection coefficients as a function of the wavelength. reflection coefficients can be calculated as a function of polarization (Figure 10), or averaged over the polarizations as shown Figure 11. The reflection coefficient appears to be largely underestimated before the 860nm gap, with 10% of reflection less than the reference measurement. But the estimation is inside the uncertainty margin after this jump. The jump is due to the impact of the diffused reflection coefficient which is the principal influencer for the global reflection coefficient, whereas the specular reflection coefficient is relatively constant (around 4) over all wave lengths, except at 870nm and 880nm, near to the sensor change.

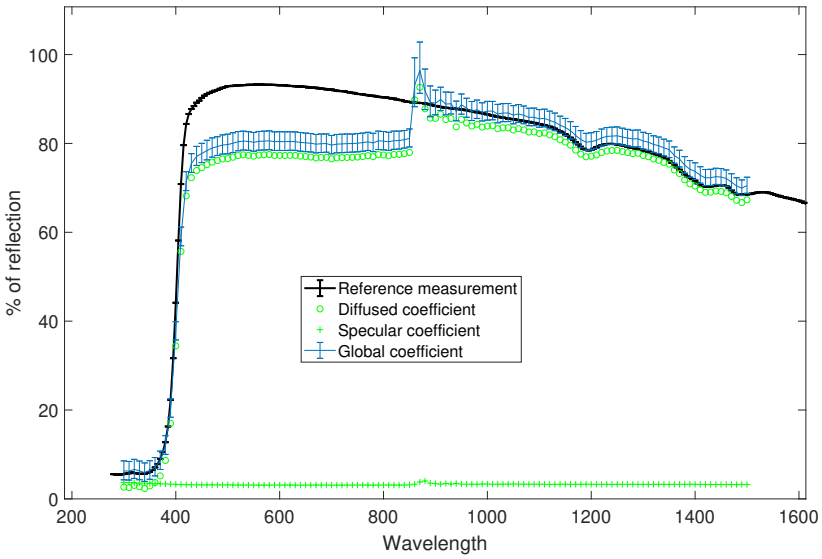

Figure 11: Global reflection coefficients for both polarization, depending of the wavelength, obtained with the BRDF model and compared to the Integrating Sphere measures.

Regarding the refractive index of the sample surface material, the trends are varied between the two polarizations. If the refractive index is almost constant for the S polarization, the refractive index is decreasing with longer wavelenght for the P polarization (Figure 12). This behavior (having a different refraction index for both polarizations) is observed for birefringing materials. However, here, the two different values come form identifying a parameter inside a model and are too far apart for the sample material to be considered as birefinging. The refractive index in the model can be forced to the same value for both polarizations and this yields a value close to 1.24 (Figure 12). Again, sharp changes around the 860nm wavelength due to sensor change are observed.

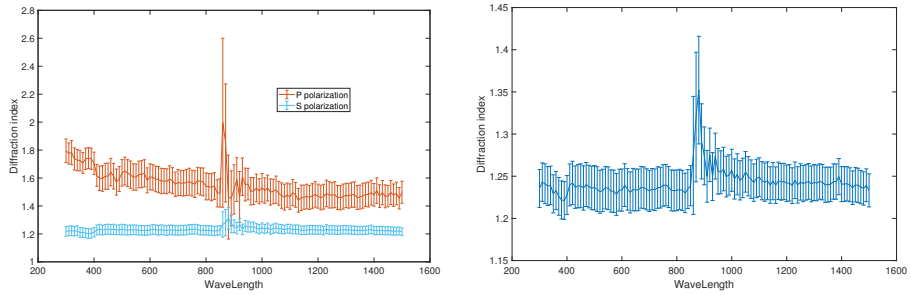

(a) Diffraction index for P and S polarizations

(b) Diffraction index obtained for both polarizations.

Figure 12: Diffraction index fitted from the ARTA measurments.

5. Discussion: using the BRDF in a solar irradiation simulation

Raybaud's thesis [11] proposes a simulation of incident irradiance with reflection models mixing specular and diffuse. As mentioned in Section 4, the reflection coefficients used in the solar irradiance models at this stage are integrated over all wavelengths. Both reflections are simulated using a Monte Carlo model coded in Matlab®. This simplified simulation assumes that the facade surfaces are lambertian (reflection coefficient of 72%) and specular (reflection coefficient of 4%). These values correspond to the values identified for the white cladding. The energy gains from specular reflections are therefore evaluated from a ray-tracing simulation taking into account only the specular part of the reflections. These contributions are visible but low (about 30W/m^2, Figure 13).

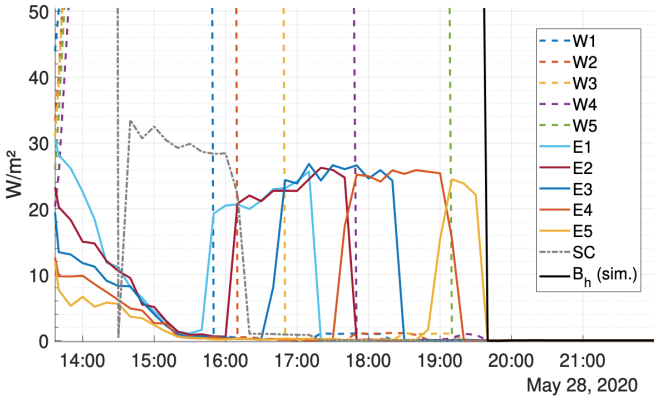

Figure 13: Energy contribution of specular reflections evaluated with a reflection coefficient of 4% corresponding to the identified value in the case of white cladding (from Raybaud [11])

The interest in making reflection models more complex in order to take into account different reflection modes seems limited, especially for large-

scale simulations. Windows can generate significant reflections at certain angles of incidence and a better understanding of the reflection patterns of materials in the urban environment could provide more information on this point. On this point, these models can also be of interest for glare and visual comfort issues. They can also help to better simulate the spectrum incident on photovoltaic modules in order to better assess their integration and camouflage into the urban landscape.

6. Conclusion

This study considers the influence of light wavelength and polarization, angle of incidence and angle of observation on the reflectance of a cladding material used for building construction. This material appears highly reflective (to the eye) at grazing angles of incidence, rising the need for a BRDF model that is able to reproduce such a behavior. Inspired by the Fresnel equations, the specular term combined with a usual diffuse term in our BRDF model are able to match the observations carried out on the ARTA device. The largest discrepancy between the reconstructed BRDF and the measurements with the integrating sphere lies in the $400-860$nm range of wavelength. Our best bet is that our calibration for this particular sensor is not accurate.

The results confirm the need to consider polarization and angular dependency when considering physical modeling of reflections, especially for angular energy distribution. This is usually done through ray-tracing algorithms, where a BRDF model is required. A new BRDF model, integrating the polarization dependence based on the Fresnel coefficients, is then proposed and validated on different samples. This model has only four parameters for each wavelength and polarization. Considering the usual split between diffuse and specular reflectance in light simulation, these four parameters can be reduced to two (diffuse and specular global reflection coefficients) keeping the same energy ratios.

With only two parameters (governing importance sampling in RT algorithms), our BRDF model can be used to verify the influence of the material properties on the energy distribution in an urban district, when the effect of such materials (sharp angular reflectance variations) is investigated.

One obvious question for further research is the wavelength and polarisation dependency of the BRDF. While it might not be of importance for energy simulations, visual integration of PV panels in the buildings' facades should strongly rely on color aspects. Then, our material sample has been tested as new. Exposure to the outdoor weather and solar rays will induce aging and maybe dirtiness, modifying the optical properties. Some further research is necessary to confirm that the specular part of the BRDF does not fade out with time.

7. Acknowledgements

The authors would like to thank the French Alternative Energies and Atomic Energy Commission (CEA) for funding this research. The study presented in this manuscript is based on the PhD thesis of Raybaud Blaise [11].

References

[1] G. Lobaccaro, F. Frontini, Solar energy in urban environment: How urban densification affects existing buildings, Energy Procedia 48 (2014) 1559–1569. URL: https://www.sciencedirect.com/science/article/pii/S187661021400438X. doi:https://doi.org/10.1016/j.egypro.2014.02.176, proceedings of the 2nd International Conference on Solar Heating and Cooling for Buildings and Industry (SHC 2013).

[2] C. Balocco, R. Calzolari, Natural light design for an ancient building: A case study, Journal of Cultural Heritage 9 (2008) 172–178. URL: http://www.sciencedirect.com/science/article/pii/S129620740800023X. doi:10.1016/j.culher.2007.07.007.

[3] M. C. Brito, S. Freitas, S. Guimarães, C. Catita, P. Redweik, The importance of facades for the solar PV potential of a mediterranean city using LiDAR data, Renewable Energy 111 (2017) 85–94. URL: http://www.sciencedirect.com/science/article/pii/S0960148117302768. doi:10.1016/j.renene.2017.03.085.

[4] E. Saretta, P. Bonomo, F. Frontini, A calculation method for the bipv potential of swiss façades at lod2.5 in urban areas: A case from ticino region, Solar Energy 195 (2020) 150–165. URL: https://www.sciencedirect.com/science/article/pii/S0038092X19311624. doi:https://doi.org/10.1016/j.solener.2019.11.062.

[5] G. Lobaccaro, S. Carlucci, S. Croce, R. Paparella, L. Finocchiaro, Boosting solar accessibility and potential of urban districts in the nordic climate: A case study in trondheim, Solar Energy 149 (2017) 347–369. URL: https://linkinghub.elsevier.com/retrieve/pii/S0038092X17302992. doi:10.1016/j.solener.2017.04.015.

[6] Z.-H. Wang, Monte carlo simulations of radiative heat exchange in a street canyon with trees, Solar Energy 110 (2014) 704–713. URL: http://www.sciencedirect.com/science/article/pii/S0038092X14004988. doi:10.1016/j.solener.2014.10.012.

[7] P. Bijl, A. Heikkilä, S. Syrjälä, A. Aarva, A. Poikonen, Modelling of sample surface temperature in an outdoor weathering test, Polymer Testing 30 (2011) 485–492. URL: http://linkinghub.elsevier.com/retrieve/pii/S014294181100047X. doi:10.1016/j.polymertesting.2011.03.009.

[8] M. Manni, G. Lobaccaro, F. Goia, A. Nicolini, F. Rossi, Exploiting selective angular properties of retro-reflective coatings to mitigate solar irradiation within the urban canyon, Solar Energy 189

(2019) 74–85. URL: http://www.sciencedirect.com/science/article/pii/S0038092X19307078. doi:10.1016/j.solener.2019.07.045.

[9] A. Vallati, L. Mauri, C. Colucci, P. Ocłoń, Effects of radiative exchange in an urban canyon on building surfaces' loads and temperatures, Energy and Buildings 149 (2017) 260–271. URL: http://www.sciencedirect.com/science/article/pii/S0378778817311076. doi:10.1016/j.enbuild.2017.05.072.

[10] M. Langovoy, G. Wubbeler, Empirical BRDF models for standard reference materials, Euramet JRP-i21 Deliverable 4.2.1 (2013) 9.

[11] B. Raybaud, Evaluation de l'impact des propriétés optiques large-bande de l'environnement sur le productible (énergie incidente) en milieu urbain, phdthesis, Université de Lyon, 2020. URL: https://tel.archives-ouvertes.fr/tel-03178836.

[12] E. A. Yafei, V. Badler, N. Badler, J. T. K. Jr, Accurate graphics BRDF material properties and illumination for dirt and mudbrick structures, in: International Conference on Cultural Heritage and New Technologies — Vienna — 2019, 2019.

[13] B. Wang, W. S. Koh, H. Liu, J. Yik, V. P. Bui, Simulation and validation of solar heat gain in real urban environments, Building and Environment 123 (2017) 261–276. URL: https://www.sciencedirect.com/science/article/pii/S0360132317302925. doi:10.1016/j.buildenv.2017.07.006.

[14] J. Yuan, K. Emura, C. Farnham, Geometrical-optics analysis of reflective glass beads applied to building coatings, Solar Energy 122 (2015) 997–1010. URL: https://www.sciencedirect.com/science/article/pii/S0038092X15005666. doi:10.1016/j.solener.2015.10.015.

[15] Y. Wu, J. H. Kämpf, J.-L. Scartezzini, Performance assessment of the BTDF data compression based on wavelet transforms in daylighting simulation, Solar Energy 190 (2019) 329–336. URL: http://www.sciencedirect.com/science/article/pii/S0038092X19307686. doi:10.1016/j.solener.2019.07.096.

[16] E. S. Lee, D. Geisler-Moroder, G. Ward, Modeling the direct sun component in buildings using matrix algebraic approaches: Methods and validation, Solar Energy 160 (2018) 380–395. URL: http://www.sciencedirect.com/science/article/pii/S0038092X17311118. doi:10.1016/j.solener.2017.12.029.

[17] J. M. Jurado, J. R. Jiménez-Pérez, L. Pádua, F. R. Feito, J. J. Sousa, An efficient method for acquisition of spec-

tral BRDFs in real-world scenarios, Computers & Graphics (2021). URL: https://www.sciencedirect.com/science/article/pii/S0097849321001850. doi:10.1016/j.cag.2021.08.021.

[18] M. Yang, W. Xu, J. Li, Z. Zhou, Y. Lu, A modified version of BRDF model based on kubelka-munk theory for coating materials, Optik 193 (2019) 162982. URL: http://www.sciencedirect.com/science/article/pii/S0030402619308599. doi:10.1016/j.ijleo.2019.162982.

[19] R. Guerrero-Lemus, R. Vega, T. Kim, A. Kimm, L. Shephard, Bifacial solar photovoltaics – a technology review, Renewable and Sustainable Energy Reviews 60 (2016) 1533–1549. URL: https://linkinghub.elsevier.com/retrieve/pii/S1364032116002768. doi:10.1016/j.rser.2016.03.041.

[20] M. Ayoub, A review on light transport algorithms and simulation tools to model daylighting inside buildings, Solar Energy 198 (2020) 623–642. URL: http://www.sciencedirect.com/science/article/pii/S0038092X20301250. doi:10.1016/j.solener.2020.02.018.

[21] C. Collin, S. Pattanaik, P. LiKamWa, K. Bouatouch, Discrete ordinate method for polarized light transport solution and subsurface BRDF computation, Computers & Graphics 45 (2014) 17–27. URL: http://www.sciencedirect.com/science/article/pii/S009784931400082X. doi:10.1016/j.cag.2014.09.002.

[22] B. T. Phong, Illumination for computer generated pictures, Communications of the ACM 18 (1975) 311–317. URL: http://portal.acm.org/citation.cfm?doid=360825.360839. doi:10.1145/360825.360839.

[23] E. P. F. Lafortune, S.-C. Foo, K. E. Torrance, D. P. Greenberg, Non-linear approximation of reflectance functions, in: Proceedings of the 24th annual conference on Computer graphics and interactive techniques - SIGGRAPH '97, ACM Press, 1997, pp. 117–126. URL: http://portal.acm.org/citation.cfm?doid=258734.258801. doi:10.1145/258734.258801.

[24] J. F. Blinn, Models of light reflection for computer synthesized pictures, SIGGRAPH Comput. Graph. 11 (1977) 192–198. URL: https://doi.org/10.1145/965141.563893. doi:10.1145/965141.563893.

[25] R. L. Cook, A reflectance model for computer graphics, ACM Transactions on Graphics 1 (1982) 18.

[26] K. E. Torrance, E. M. Sparrow, Theory for off-specular reflection from roughened surfaces*, Journal of the Optical Society of America 57 (1967) 1105. URL: https://www.osapublishing.org/abstract.cfm?URI=josa-57-9-1105. doi:10.1364/JOSA.57.001105.

[27] M. Born, E. Wolf, A. B. Bhatia, P. C. Clemmow, D. Gabor, A. R. Stokes, A. M. Taylor, P. A. Wayman, W. L. Wilcock, Principles of Optics: Electromagnetic Theory of Propagation, Interference and Diffraction of Light, 7 ed., Cambridge University Press, 1999. doi:10.1017/CBO9781139644181.

[28] C. Kelemen, L. Szirmay-Kalos, A microfacet based coupled specular-matte brdf model with importance sampling, In Eurographics Short Presentations 25 (2001).

[29] P. Nijnatten, Optical analysis of coatings by variable angle spectrophotometry, Thin Solid Films 516 (2007) 4553–4557. URL: https://www.sciencedirect.com/science/article/pii/S0040609007009145. doi:10.1016/j.tsf.2007.06.027.

[30] D. Xie, T. Cheng, Y. Wu, H. Fu, R. Zhong, J. Yu, Polarized reflectances of urban areas: Analysis and models, Remote Sensing of Environment 193 (2017) 29–37. URL: http://www.sciencedirect.com/science/article/pii/S0034425717300858. doi:10.1016/j.rse.2017.02.026.

[31] R. Montes, C. Ureña, An Overview of BRDF Models, Technical Report Technical Report LSI-2012-001, University of Granada, Granada, Spain, 2012.

[32] W. Shi, J. Zheng, Y. Li, X. Li, Q. An, Measurement and modeling of bidirectional reflectance distribution function (BRDF) on cutting surface based on the coaxial optical microscopic imaging, Optik 170 (2018) 278–286. URL: http://www.sciencedirect.com/science/article/pii/S0030402618306053. doi:10.1016/j.ijleo.2018.04.111.

[33] H. Kumar, J. Ramkumar, K. S. Venkatesh, Surface texture evaluation using 3d reconstruction from images by parametric anisotropic BRDF, Measurement 125 (2018) 612–633. URL: http://www.sciencedirect.com/science/article/pii/S0263224118303725. doi:10.1016/j.measurement.2018.04.090.